# Limited formation of isoprene epoxydiols-derived secondary organic aerosol under NOx-rich environments in Eastern China

Yunjiang Zhang, Lili Tang, Yele Sun, Olivier Favez, Francesco Canonaco, Alexandre Albinet, Florian Couvidat, Dantong Liu, John Jayne, Zhuang Wang, et al.

# Limited formation of isoprene epoxydiols–derived secondary organic aerosol (IEPOX-SOA) under $NO_x$-rich environments in Eastern China

Yunjiang Zhang[1-4], Lili Tang[1,2], Yele Sun[5], Olivier Favez[3], Francesco Canonaco[6], Alexandre Albinet[3], Florian Couvidat[3], Dantong Liu[7], John T. Jayne[8], Zhuang Wang[1], Philip L. Croteau[8], Manjula R. Canagaratna[8], Hong-cang Zhou[1], André S. H. Prévôt[6], Douglas R. Worsnop[8]

[1]Jiangsu Collaborative Innovation Center of Atmospheric Environment and Equipment Technology, Nanjing University of Information Science and Technology, Nanjing 210044, China

[2]Jiangsu Environmental Monitoring Center, Nanjing 210036, China

[3]Institut National de l'Environnement Industriel et des Risques, Verneuil en Halatte, 60550, France

[4]Laboratoire des Sciences du Climat et de l'Environnement, CNRS-CEA-UVSQ, Université Paris-Saclay, Gif sur Yvette, 91191, France

[5]State Key Laboratory of Atmospheric Boundary Layer Physics and Atmospheric Chemistry, Institute of Atmospheric Physics, Chinese Academy of Sciences, Beijing 100029, China

[6]Laboratory of Atmospheric Chemistry, Paul Scherrer Institute, Villigen PSI 5232, Switzerland

[7]Centre for Atmospheric Science, School of Earth, Atmospheric and Environmental Sciences, University of Manchester, Manchester M13 9PL, UK

[8]Aerodyne Research, Inc., Billerica, Massachusetts 01821, United States

Correspondence to: L. Tang (lily3258@163.com) and Y. Sun (sunyele@mail.iap.ac.cn)

## Key points

- First real-time characterization of IEPOX-SOA in Eastern China
- The formation of IEPOX-SOA under $NO_x$-rich environments is limited
- Source analysis elucidated the interactions between biogenic and anthropogenic emissions

## Abstract

Secondary organic aerosol (SOA) derived from isoprene epoxydiols (IEPOX) have potential impacts on regional air quality and climate, yet is poorly characterized under $NO_x$-rich ambient environments. We report the first real-time characterization of IEPOX-derived SOA (IEPOX-SOA) in Eastern China in summer 2013 using comprehensive ambient measurements, along with model analysis. The ratio of IEPOX-SOA to isoprene high-$NO_x$ SOA precursors, e.g., methyl vinyl ketone and methacrolein, and the reactive uptake potential of IEPOX were lower than those generally observed in regions with prevailing biogenic emissions, low $NO_x$ levels and high particle acidity, elucidating the suppression of IEPOX-SOA formation under $NO_x$-rich environments. IEPOX-SOA showed high potential source regions to the south with large biogenic emissions, illustrating that the interactions between biogenic and anthropogenic emissions might have played an important role in affecting the formation of IEPOX-SOA in polluted environments in Eastern China.

## 1. Introduction

Isoprene (2-methyl-1,3-butadiene, $C_5H_8$) is the most abundant non-methane hydrocarbon compound emitted in the Earth's atmosphere [*Guenther et al.*, 2012]. Oxidation of isoprene can form secondary organic aerosol (SOA), which has potential impacts on human health [*Y-H Lin et al.*, 2016], air quality [*von Schneidemesser et al.*, 2011], and regional climate [*Guenther et al.*, 2012]. Isoprene epoxydiols (IEPOX), a key gas-phase oxidation product of isoprene, plays an especially significant role in ambient isoprene SOA formation [*Surratt et al.*, 2010]. For example, IEPOX-SOA can account for more than 30 % of total organic aerosol (OA) in the Amazonian forest [*Chen et al.*, 2015] and the southeastern US [*Budisulistiorini et al.*, 2013; *Hu et al.*, 2015]. Although IEPOX-derived SOA has been widely identified in isoprene-rich environments [*Hu et al.*, 2015], e.g., the densely forested regions [*Chen et al.*, 2015], there is still a great challenge to improve modeling frameworks for evaluating its influence on air quality and climate change, due to the lack of observed IEPOX-SOA under polluted urban environments.

The hydroperoxyl radicals ($HO_2$) pathway has been recognized as a dominant mechanism to form IEPOX-SOA through acid-catalyzed multiphase chemistry under low-$NO_x$ conditions [*Archibald et al.*, 2011; *Surratt et al.*, 2010]. The formation of IEPOX-SOA via $HO_2$-pathway can be shifted to the NO and $NO_2$ pathway under high-$NO_x$ conditions, producing gas-phase methyl vinyl (MVK) and methacrolein (MACR), the first-generation photo-oxidation products of isoprene [*Surratt et al.*, 2010; *Surratt et al.*, 2006]. Further oxidation of MACR leads to the formation of either methacrylic acid epoxide (MAE) [*Y-H Lin et al.*, 2013a] or hydroxymethyl-methyl-α-lactone (HMML) [*Nguyen et al.*, 2015]. There is a direct chemical evidence for MAE in the gas phase [*Y H Lin et al.*, 2013b] although its reactive uptake chemistry is fairly slow under acidic conditions [*Riedel et al.*, 2015]. *Nguyen et al.* [2015] recently suggested that HMML likely leads to the formation of most SOA from isoprene under high-$NO_x$ conditions. The isoprene-SOA related tracers, e.g., $C_5$-alkene triols, 2-methylglyceric acid, and 2-methyltetrols (MTLs), have been mainly detected so far via filter-based analytical approaches [*Ding et al.*, 2016; *Rattanavaraha et al.*, 2016]. Recent studies conducted with Aerodyne aerosol mass spectrometer (AMS) [*Canagaratna et al.*, 2007] and/or aerosol chemical speciation monitor (ACSM) [*Ng et al.*, 2011], followed by positive matrix factorization (PMF) analysis [*Paatero and Tapper*, 1994], have been shown to be capable of quantifying IEPOX-SOA [*Budisulistiorini et al.*, 2013; *Hu et al.*, 2015]. However, despite extensive efforts in characterization of IEPOX-SOA formation chemistry in IEPOX-rich areas, only few studies have been conducted in densely anthropogenic-dominated emission regions with high $NO_x$ levels, especially in East Asia.

Eastern China has been suffering from severe fine particle pollution during the past decade [*Guo et al.*, 2014; *R J Huang et al.*, 2014]. The contribution of SOA to fine particles was found to be substantial in this region, mainly due to high anthropogenic emissions and rapid formation of secondary aerosols [*Sun et al.*, 2014; *Y Zhang et al.*, 2015a]. Recent studies also showed significant influences of biogenic emissions on air quality in this region [*Geng et al.*, 2011]. Therefore, this region provides a unique environment to investigate the interaction between anthropogenic activities and biogenic emissions, and its impacts on atmospheric IEPOX-SOA chemistry. In this study, an ACSM was deployed in a polluted urban city (i.e., Nanjing in Eastern China) in summer 2013 for real-time characterization of aerosol particle composition and sources. Here we report the identification and quantification of an IEPOX-SOA factor via PMF analysis of OA spectra, and investigate the potential of the IEPOX reactive kinetics uptake on particles influenced by anthropogenic emissions using an

acid-catalyzed mechanism model [*Eddingsaas et al.*, 2010]. Also, the potential sources of IEPOX-SOA are illustrated using potential source contribution function (PSCF) [*Polissar et al.*, 2001] and non-parametric wind regression (NWR) [*Henry et al.*, 2009] analysis.

## 2. Experiment

### 2.1 Sampling site and measurements

All the measurements were conducted on the roof of a six-story building (approximately 18 m above the ground) at Jiangsu Environment Monitoring Center in urban Nanjing (32’03 °N, 118’46 °E). This sampling site is extensively described in supporting information (Sect. S1). Briefly, it is a typical urban site mainly influenced by anthropogenic activities, such as traffic and cooking emissions [*Y J Zhang et al.*, 2015b]. Some industries [*Wang et al.*, 2016], like power, iron-steel, and oil refineries, are located approximately 15 - 25 km to the north and south. The spatial distributions of isoprene emissions (Fig. S1) suggest that the sampling site is subject to influences from mixed anthropogenic and biogenic emissions. The non-refractory submicron aerosol (NR-$PM_1$) species, including OA, sulfate, nitrate, ammonium and chloride, were measured on-line using the ACSM with a ~30 min time resolution. A more detailed description of the ACSM can be found elsewhere [*Ng et al.*, 2011; *Sun et al.*, 2012]. The oxidation products of isoprene, MVK and MACR, were measured every hour using an on-line Gas Chromatography-MS/Flame Ionization Detector (GC-MS/FID) system that has been described by *Yuan et al.* [2012]. Particle number size distributions from ~13 nm to 600 nm were measured using a scanning mobility particle sizer that consists of a differential mobility analyzer (TSI Model 3081) and a condensation particle counter (TSI Model 3775). Gaseous species, including NO-$NO_2$-$NO_x$ (model 42i), $O_3$ (model 49i), and $SO_2$ (model 43i), were measured using collocated Thermo Scientific gas analyzers. Gas-phase ammonia ($NH_3$) was measured by a Monitor for Aerosols and Gases in Air (MARGA). The total $PM_1$ and $PM_{2.5}$ mass concentrations were measured using two Met One systems (BAM-1020). In addition, meteorological parameters, such as temperature (*T*), relative humidity (RH), wind speed (WS), and wind direction (WD), were obtained from a meteorological station at the same location. A summary of the meteorological conditions is given in Table S1.

**2.2 Data analysis.**

The ACSM data were analyzed by standard data analysis software [*Allan et al.*, 2004] written in IGOR Pro. The collection efficiency (CE) values used for the ACSM data analysis were based on the composition-dependent CE = *max* (0.45, 0.0833 + 0.9167 × ANMF) [*Middlebrook et al.*, 2012], in which ANMF is the mass fraction of $NH_4NO_3$ in $PM_1$. Ionization efficiency (IE) and relative ionization efficiencies (RIEs) were calibrated with pure ammonium nitrate (see Sect. S1) following the procedures in *Ng et al.* [2011]. The satisfactory inter-comparison results between NR-$PM_1$ and total $PM_1$ and $PM_{2.5}$ can be found in Figure S3.

PMF with ME-2 algorithm was performed on the ACSM OA mass spectra, and the results were then carefully evaluated using the Source Finder (SoFi) toolkit [*Canonaco et al.*, 2013]. Four OA factors were identified, including three oxygenated factors, i.e., IEPOX-SOA, a less oxidized oxygenated OA (LO-OOA), and a more oxidized OOA (MO-OOA), and a primary OA factor (hydrocarbon-like OA, HOA). The detailed reasons for the selection of this 4-factor solution can be found in Supporting Information (Sect. S2).

Particle liquid water content (LWC) associated with inorganic species, and particle acidity (pH) were predicted using a thermodynamic model (ISORROPIA-II) [*Fountoukis and Nenes*, 2007], along with the "forward mode" for metastable aerosol. A modified resistor model [*Gaston et al.*, 2014] based on acid-catalyzed mechanism [*Eddingsaas et al.*, 2010] was applied for modeling the potential of IEPOX reactive uptake ($\gamma_{IEPOX}$) and the first-order reaction rate constant in the aqueous phase ($k_{aq}$). More details are given in Supporting Information (Sect. S3).

48-h backward trajectories were obtained from the Hybrid Single-Particle Lagrangian Integrated Trajectory (HYSPLIT) model [*Draxler*, 2003], developed by National Oceanic and Atmospheric Administration (NOAA)/Air Resources Laboratory (ARL), for simulating air mass arrivals at 100 m altitude (a.g.l.) with 1 h resolution. PSCF and NWR analysis in this study were using the ZeFir toolkit [*Petit et al.*, 2017]. PSCF was performed on the combined measurements and the corresponding air masses histories from HYSPLIT outputs (see details in section S3). NWR was also performed on OA factors, NR-$PM_1$ species, and gas-phase tracers. In brief, NWR is a source-to-receptor model to estimate wind-dependent sources of atmospheric pollutants. The percent of a given pollutant which is originated from a specific wind sector can be identified and quantified using kernel smoothing methods [*Henry et al.*, 2009].

## 3. Results and discussion

Figure 1 shows the temporal variations of meteorological parameters (*T*, RH, WD, and air masses history), gas-phase species ($O_3$, $NO_2$, isoprene, and MVK+MACR), and IEPOX-SOA and sulfate. The average mixing ratio of $NO_x$ is 21.4 ppb, which is about 20 times higher than that (0.1 – 2 ppb) at Look Rock, Tennessee in the southeastern US where high IEPOX-SOA concentrations were reported [*Budisulistiorini et al.*, 2015]. Also, the average NR-$PM_1$ mass loading is approximately 3 times higher, indicating an environment with substantial anthropogenic emissions in this study. The three OOA factors dominate OA for the entire study, on average accounting for 78.0% of the total OA mass. This is consistent with the results from a previous study in Shanghai, a megacity near Nanjing, showing a predominance of SOA over primary aerosols during the summer season [*X F Huang et al.*, 2012]. The average IEPOX-SOA concentration is 0.33 ± 0.19 μg/$m^3$ for the entire study, accounting for 3.8% of the total OA. Compared to the IEPOX-rich regions, such as Yorkville (4 μg/$m^3$), Georgia (3 μg/$m^3$), and Jefferson (2 μg/$m^3$) in the southeastern US [*Xu et al.*, 2015a], IEPOX-SOA shows a much smaller average concentration under polluted urban environments in Eastern China.

The formation of isoprene peroxy radicals (ISOPOO) is derived from isoprene reaction with OH radical, but their fate is dominated by NO-$HO_2$ conditions in the atmosphere [*Liu et al.*, 2016; *Paulot et al.*, 2009]. ISOPOO mainly reacts with NO and produces $NO_2$ and MVK and MACR under NO-dominant conditions [*Liu et al.*, 2016; *Surratt et al.*, 2010]. It can also react with $HO_2$ radicals to dominantly produce hydroxyhydroperoxides (ISOPOOH) [*Paulot et al.*, 2009]. As shown in Figure 2a, IEPOX-SOA, as well as $O_x$ and MVK+MACR concentrations are increasing with the [$NO_2$]/[NO] ratio, implying that enhanced $O_3$ and/or OH concentrations might increase both isoprene oxidation products via $HO_2$ and NO pathways. Some contributions of MACR and MVK could come from decomposition of other products (such as ISOPOOH) [*St. Clair et al.*, 2016], which might be another potential reason for the positive relationship between MVK + MACR and IEPOX-SOA. However, the formation of IEPOX via $RO_2$+$HO_2$ pathway could be suppressed due to the high ambient NO loadings. In addition, *Jacobs et al.* [2014] demonstrated that further oxidation of the first-generation isoprene hydroxynitrates in the presence of high NO yielded much lower IEPOX than that from the oxidation of low-$NO_x$ ISOPOOH products [*Paulot et al.*, 2009]. Thus $RO_2$+NO pathway might also produce IEPOX under high $NO_x$ conditions, and thereby to form a very small fraction of ambient IEPOX-SOA [*Jacobs et al.*, 2014; *Xu et al.*, 2016].

The increase of IEPOX-SOA is much higher during high $O_3$ episode compared to the entire period (Fig. 2a), which could be explained by the formation and subsequent isoprene photooxidation of ISOPOOH, forming IEPOX-SOA via $HO_2$-pathway. Furthermore, recent works showed that MTLs, a component of IEPOX-SOA for isoprene low-$NO_x$ pathway SOA tracers, can be formed via the reaction of isoprene with $O_3$ in the presence of acidic aerosols [*Rattanavaraha et al.*, 2016; *Riva et al.*, 2016]. Although it remains unclear to quantify exactly isoprene with $O_3$ reactions to yield MTLs, the products from these reactions are certainly undergoing acid-catalyzed multiphase chemistry to yield MTLs that could contribute to IEPOX-SOA burden. Although the isoprene mixing ratio in this study is approximately 4 times lower than those in the southeastern US, the average isoprene emission flux seems to be quite similar (~ 1.7-1.9 mg $m^{-2}$ $hr^{-1}$) for both area, as obtained from the model (Fig. S11). The average ratio of [MVK+MACR]/[Isoprene] is 1.31 in this study, which is approximately 3 times than that in the southeastern US (Fig. S12) [*Xiong et al.*, 2015]. However, the [IEPOX-SOA]/[MVK+MACR] is nearly 5 times lower than that under relatively low-$NO_x$ environments during summertime 2013 in the southeastern US [*Budisulistiorini et al.*, 2015; *Xiong et al.*, 2015; *Xu et al.*, 2015a]. This is likely due to the rapid oxidation processes of isoprene to largely yield $NO_x$-pathway isoprene oxidation products under $NO_x$-rich environments. For example, once isoprene emitted into the atmosphere, it can be rapidly oxidized by OH radical [*Paulot et al.*, 2009], and forms MVK and MACR [*Liu et al.*, 2016; *Surratt et al.*, 2010; *Surratt et al.*, 2006]. These results suggest that $RO_2$ + NO reaction pathway might dominate the isoprene SOA chemistry under $NO_x$-rich environments in Eastern China although both regimes of $RO_2$ + $HO_2$ and $RO_2$ + NO are prevalent. This may also constrain the conversion efficiency of isoprene to gas-phase IEPOX, leading to an impediment of IEPOX-SOA formation.

To investigate the effects of particle LWC, particle acidity ($H^+_{(aq)}$), and sulfate on IEPOX-SOA formation, a multivariate linear regression analysis was performed following the procedures in *Xu et al.* [2015a] (Table S2). Sulfate presents a statistically significant positive relationship ($P < 0.0001$) with IEPOX-SOA, and IEPOX-SOA is correlated well with the total particle surface area ($r = 0.78$, Fig. 3a). We also note that the ratio of IEPOX-SOA to MVK+MACR is enhanced during periods with higher sulfate loadings (Fig. 2b). These results suggest that IEPOX-SOA formation in urban Nanjing is likely mediated by pre-existing sulfate particles (i.e., nucleophile and/or salting-in effect) which may facilitate the ring-opening reactions of IEPOX and provide particle area required for IEPOX reactive

uptake [*Y-H Lin et al.*, 2012; *Xu et al.*, 2015a]. However, the efficiency of IEPOX-SOA formation might be lower than that in the southeastern US [*Xu et al.* 2015a] as indicated by the more than 10 times lower regression slope (0.03 vs. 0.42). Interestingly, particle water shows a statistically significant relationship ($P < 0.0001$) with IEPOX-SOA, but with a negative regression coefficient (– 0.005) (Table S2). As shown in Fig. 4, $k_{aq}$, indicative of aqueous-phase reaction rate constant of IEPOX [*Eddingsaas et al.*, 2010; *Gaston et al.*, 2014], shows a negative relationship with particle LWC, supporting that particle water may reduce aqueous-phase reaction rate by decreasing aerosol acidity and nucleophile e.g., $SO_4^{2-}{}_{(aq)}$, concentrations and suppressing the IEPOX kinetic uptake due to the weaker ionic strength and salting-in effect [*Xu et al.*, 2015a]. Thus, particle water increases in this study still keep within limits of IEPOX-SOA formation.

$H^+_{(aq)}$ does not show a statistically significant correlation with IEPOX-SOA (Table S2), likely due to the fact that aerosol acidity doesn't vary as much as sulfate loadings (Fig. S13). This result is consistent with previous field observations made in the southeastern US [*Budisulistiorini et al.*, 2015; *Y H Lin et al.*, 2013b; *Rattanavaraha et al.*, 2016; *Xu et al.*, 2015a]. The average concentrations of bisulfate $HSO_4^-$ and $H^+_{(aq)}$ are 0.02 mol/L and 0.01 mol/L (corresponding to an average pH = 2.6), respectively, indicating significant lower particle acidity levels compared with those in the southeastern US [*Hu et al.*, 2015]. This could be due to the neutralization effect by the abundant ammonium (Fig. S4). As shown in Fig. 3b, IEPOX-SOA shows independent variations on LWC and $H^+_{(aq)}$, but was strongly associated sulfate variations, which is consistent with the results reported by *Xu et al.* [2015a]. This might be due to the competition between IEPOX uptake to particles and subsequent aqueous-phase reactions [*Xu et al.*, 2016]. For example, Gaston et al. (2014) found that the reactive uptake of *trans-β*-IEPOX is driven by ring-opening chemistry under the condition of pH ≥ 1, but not acid catalysis. In addition, aerosol acidity (pH <2) is needed to make IEPOX uptake competitive with other potential atmospheric loss process of IEPOX [*Gaston et al.*, 2014], such as IEPOX + OH [*Bates et al.*, 2014] or IEPOX deposition [*Eddingsaas et al.*, 2010]. Therefore, the results above further support that the IEPOX-SOA formation is likely dominantly affected by the sulfate particles rather than particle acidity and/or particle water in this study.

The average value of $\gamma_{IEPOX}$ is $1.57 \times 10^{-4}$ ranging from $1.03 \times 10^{-5}$ to $5.10 \times 10^{-4}$, which is overall consistent with those from laboratory experiments ($2 - 6.5 \times 10^{-4}$) [*Gaston et al.*, 2014; *Riedel et al.*, 2015] with ammonium sulfate as aerosol seeds. However, these values are approximately two orders of magnitude lower than those under high particle acidity conditions (e.g., bisulfate as seeds) [*Gaston et al.*, 2014; *Riedel et al.*, 2015] and in sulfur-rich plumes [*Xu et al.*, 2016]. Therefore, the lower $\gamma_{IEPOX}$ might be mainly due to the correspondingly lower particle acidity in this study. The pseudo-first-order heterogeneous reaction rate efficient ($k_{het}$) for IEPOX uptake on particles depends on $\gamma_{IEPOX}$ and particle surface area [*Gaston et al.*, 2014]. The average $k_{het}$ is $7.12 \times 10^{-8}$ in this study, which is significantly lower than that was reported in the sulfur-rich plumes [*Xu et al.*, 2016]. These results indicate that aqueous-phase reaction is not sufficiently fast due to low particle acidity and low probability of IEPOX reactive uptake in this study. To quantitatively evaluate the effects of particle acidity on $k_{het}$, we further calculated $k_{het}$ ($k_{het,\ new}$) using a new $\gamma_{IEPOX}$ by increasing the $H^+_{(aq)}$ concentration by a factor of 10 (Fig. 4), a value close to that in the power-plant plumes in Scherer in the southeastern US [*Xu et al.*, 2016]. We found that approximately 90% (= $[(k_{het,\ new} - k_{het}) / k_{het,\ new}] \times 100$) of the $k_{het}$ enhancement can be explained by the increase of particle acidity. Therefore, our results illustrate that the reactive uptake chemistry might be one of the major factors in the suppression of IEPOX-SOA formation under polluted environments in Eastern China. In addition, a very recent study also found the limited formation of IEPOX-SOA under high NO plumes near Manaus, Brazil in the Amazon [*de Sá et al.*, 2016], which is consistent with our conclusions.

As shown in Figure 5, IEPOX-SOA shows an evident wind sector gradient, with the highest concentrations in association with winds from the south. Such wind sector dependence of IEPOX-SOA is remarkably consistent with the spatial distribution of biogenic emissions in Eastern China (Fig. S1). Moreover, the high potential source areas for IEPOX-SOA, mainly located at the south of Nanjing, were consistent with those with high isoprene loadings (Fig. S1) and gas-phase IEPOX in Eastern China [*Hu et al.*, 2015]. In addition, gas-phase MVK+MACR also shows similar wind sector dependence (Fig. S15) and potential sources areas (Fig. S16) as IEPOX-SOA. In contrast, anthropogenic emissions related gas-phase species, such as $SO_2$ and $NO_2$, present different wind sector gradients (Fig. S15). For example, $SO_2$ shows a more regional character with high concentration associated with winds from the north-northwest and the south-southwest. The wide potential source areas for sulfate (mostly formed by cloud processing of $SO_2$) also indicate a regional origin

[*Sun et al.*, 2014]. These results suggest that mixing of biogenic and anthropogenic air masses during regional transport of biogenic emissions from their emissions-rich regions impacts the formation of IEPOX-SOA under polluted urban environments.

## 4. Implications

We have identified an IEPOX-SOA factor in polluted environments in Eastern China. Our results showed that the IEPOX-SOA formation was more sensitive to ring-opening chemistry mediated by aerosol sulfate along with enhanced particle surface area rather than acid catalysis chemistry, and the suppression of IEPOX-SOA formation was mainly caused by the low IEPOX reactive uptake rate and the NO-dominant gas-phase chemistry with less production of IEPOX-SOA precursors. Considering that IEPOX-SOA shows a considerable contribution to OA in the global Earth, and might have potential impacts on radiative forcing and human health, a long-term characterization of IEPOX-SOA in highly polluted environment is urgently needed. Our results also show that regional climate models need to consider the impacts of anthropogenic $NO_x$, $SO_2$ and $NH_3$ on the isoprene SOA formation via low-$NO_x$ pathway in highly polluted environments to have a better evaluation of the radiative forcing of IEPOX-SOA.

## Acknowledgments

This work was supported by Natural Science Foundation of China (D0512/91544231). We would like to thank the supports from INERIS. Y. Zhang acknowledges the PhD Scholarship from the China Scholarship Council (CSC).

## References


Allan, J. D., et al. (2004), A generalised method for the extraction of chemically resolved mass spectra from Aerodyne aerosol mass spectrometer data, *J. Aerosol Sci.*, *35*(7), 909-922, doi:10.1016/j.jaerosci.2004.02.007.

Archibald, A. T., et al. (2011), Impacts of HOx regeneration and recycling in the oxidation of isoprene: Consequences for the composition of past, present and future atmospheres, *Geophys. Res. Lett.*, *38*(5), doi:10.1029/2010GL046520.

Bates, K. H., J. D. Crounse, J. M. St. Clair, N. B. Bennett, T. B. Nguyen, J. H. Seinfeld, B. M. Stoltz, and P. O. Wennberg (2014), Gas Phase Production and Loss of Isoprene Epoxydiols, *The Journal of Physical Chemistry A*, *118*(7), 1237-1246, doi:10.1021/jp4107958.

Budisulistiorini, S. H., et al. (2013), Real-time continuous characterization of secondary organic aerosol derived from isoprene epoxydiols in downtown Atlanta, Georgia, using the Aerodyne Aerosol Chemical Speciation Monitor, *Environ. Sci. Technol.*, *47*(11), 5686-5694, doi:10.1021/es400023n.

Budisulistiorini, S. H., et al. (2015), Examining the effects of anthropogenic emissions on isoprene-derived secondary organic aerosol formation during the 2013 Southern Oxidant and Aerosol Study (SOAS) at the Look Rock, Tennessee ground site, *Atmos. Chem. Phys.*, *15*(15), 8871-8888, doi:10.5194/acp-15-8871-2015.

Canagaratna, M. R., et al. (2007), Chemical and microphysical characterization of ambient aerosols with the aerodyne aerosol mass spectrometer, *Mass Spectrom. Rev.*, *26*(2), 185-222, doi:10.1002/mas.20115.

Canonaco, F., M. Crippa, J. G. Slowik, U. Baltensperger, and A. S. H. Prévôt (2013), SoFi, an IGOR-based interface for the efficient use of the generalized multilinear engine (ME-2) for the source apportionment: ME-2 application to aerosol mass spectrometer data, *Atmos. Meas. Technol.*, *6*(12), 3649-3661, doi:10.5194/amt-6-3649-2013.

Chen, Q., et al. (2015), Submicron particle mass concentrations and sources in the Amazonian wet season (AMAZE-08), *Atmos. Chem. Phys.*, *15*(7), 3687-3701, doi:10.5194/acp-15-3687-2015.

de Sá, S. S., et al. (2016), Influence of urban pollution on the production of organic particulate matter from isoprene epoxydiols in central Amazonia, *Atmos. Chem. Phys. Discuss.*, *2016*, 1-58, doi:10.5194/acp-2016-1020.

Ding, X., Q.-F. He, R.-Q. Shen, Q.-Q. Yu, Y.-Q. Zhang, J.-Y. Xin, T.-X. Wen, and X.-M.

Wang (2016), Spatial and seasonal variations of isoprene secondary organic aerosol in China: Significant impact of biomass burning during winter, *Sci. Rep.* , *6*, 20411.

Draxler, R. R., Rolph, G.D., (2003), HYSPLIT (HYbrid Single-Particle Lagrangian Integrated Trajectory) Model Access via NOAA ARL READY Website. NOAA Air Resources Laboratory, Silver Spring, MD. http://www.arl.noaa.gov/ready/hysplit4.html.

Eddingsaas, N. C., D. G. VanderVelde, and P. O. Wennberg (2010), Kinetics and Products of the Acid-Catalyzed Ring-Opening of Atmospherically Relevant Butyl Epoxy Alcohols, *The Journal of Physical Chemistry A*, *114*(31), 8106-8113, doi:10.1021/jp103907c.

Fountoukis, C., and A. Nenes (2007), ISORROPIA II: a computationally efficient thermodynamic equilibrium model for K+- Ca2+ - Mg2+-NH4+ - Na+ - SO42- - NO3- - Cl- - H2O aerosols, *Atmos. Chem. Phys.*, *7*(17), 4639-4659, doi:10.5194/acp-7-4639-2007.

Gaston, C. J., T. P. Riedel, Z. Zhang, A. Gold, J. D. Surratt, and J. A. Thornton (2014), Reactive Uptake of an Isoprene-Derived Epoxydiol to Submicron Aerosol Particles, *Environ. Sci. Technol.*, *48*(19), 11178-11186, doi:10.1021/es5034266.

Geng, F., X. Tie, A. Guenther, G. Li, J. Cao, and P. Harley (2011), Effect of isoprene emissions from major forests on ozone formation in the city of Shanghai, China, *Atmos. Chem. Phys.*, *11*(20), 10449-10459, doi:10.5194/acp-11-10449-2011.

Guenther, A. B., X. Jiang, C. L. Heald, T. Sakulyanontvittaya, T. Duhl, L. K. Emmons, and X. Wang (2012), The Model of Emissions of Gases and Aerosols from Nature version 2.1 (MEGAN2.1): an extended and updated framework for modeling biogenic emissions, *Geosci. Model Dev.*, *5*(6), 1471-1492, doi:10.5194/gmd-5-1471-2012.

Guo, S., et al. (2014), Elucidating severe urban haze formation in China, *Proc. Natl. Acad. Sci. U.S.A.*, *111*(49), 17373-17378, doi:10.1073/pnas.1419604111.

Henry, R., G. A. Norris, R. Vedantham, and J. R. Turner (2009), Source Region Identification Using Kernel Smoothing, *Environ. Sci. Technol.*, *43*(11), 4090-4097, doi:10.1021/es8011723.

Hu, W. W., et al. (2015), Characterization of a real-time tracer for isoprene epoxydiols-derived secondary organic aerosol (IEPOX-SOA) from aerosol mass spectrometer measurements, *Atmos. Chem. Phys.*, *15*(20), 11807-11833, doi:10.5194/acp-15-11807-2015.

Huang, R. J., et al. (2014), High secondary aerosol contribution to particulate pollution during haze events in China, *Nature*, *514*(7521), 218-222, doi:10.1038/nature13774.

Huang, X. F., L. Y. He, L. Xue, T. L. Sun, L. W. Zeng, Z. H. Gong, M. Hu, and T. Zhu (2012), Highly time-resolved chemical characterization of atmospheric fine particles during 2010 Shanghai World Expo, *Atmos. Chem. Phys.*, *12*(11), 4897-4907, doi:10.5194/acp-12-4897-2012.

Jacobs, M. I., W. J. Burke, and M. J. Elrod (2014), Kinetics of the reactions of isoprene-derived hydroxynitrates: gas phase epoxide formation and solution phase hydrolysis, *Atmos. Chem. Phys.*, *14*(17), 8933-8946, doi:10.5194/acp-14-8933-2014.

Lin, Y.-H., M. Arashiro, E. Martin, Y. Chen, Z. Zhang, K. G. Sexton, A. Gold, I. Jaspers, R. C. Fry, and J. D. Surratt (2016), Isoprene-Derived Secondary Organic Aerosol Induces the Expression of Oxidative Stress Response Genes in Human Lung Cells, *Environ. Sci. Technol. Lett.*, *3*(6), 250-254, doi:10.1021/acs.estlett.6b00151.

Lin, Y.-H., et al. (2013a), Epoxide as a precursor to secondary organic aerosol formation from isoprene photooxidation in the presence of nitrogen oxides, *Proc. Natl. Acad. Sci. U.S.A.*, *110*(17), 6718-6723, doi:10.1073/pnas.1221150110.

Lin, Y.-H., et al. (2012), Isoprene Epoxydiols as Precursors to Secondary Organic Aerosol Formation: Acid-Catalyzed Reactive Uptake Studies with Authentic Compounds, *Environ. Sci. Technol.*, *46*(1), 250-258, doi:10.1021/es202554c.

Lin, Y. H., E. M. Knipping, E. S. Edgerton, S. L. Shaw, and J. D. Surratt (2013b), Investigating the influences of SO2 and NH3 levels on isoprene-derived secondary organic aerosol formation using conditional sampling approaches, *Atmos. Chem. Phys.*, *13*(16), 8457-8470, doi:10.5194/acp-13-8457-2013.

Liu, Y., et al. (2016), Isoprene photochemistry over the Amazon rainforest, *Proc. Natl. Acad. Sci. U.S.A.*, *113*(22), 6125-6130, doi:10.1073/pnas.1524136113.

Middlebrook, A. M., R. Bahreini, J. L. Jimenez, and M. R. Canagaratna (2012), Evaluation of Composition-Dependent Collection Efficiencies for the Aerodyne Aerosol Mass Spectrometer using Field Data, *Aerosol Sci. Technol.*, *46*(3), 258-271, doi:10.1080/02786826.2011.620041.

Ng, N. L., et al. (2011), An Aerosol Chemical Speciation Monitor (ACSM) for Routine Monitoring of the Composition and Mass Concentrations of Ambient Aerosol, *Aerosol Sci. Technol.*, *45*(7), 780-794, doi:10.1080/02786826.2011.560211.

Nguyen, T. B., et al. (2015), Mechanism of the hydroxyl radical oxidation of methacryloyl peroxynitrate (MPAN) and its pathway toward secondary organic aerosol formation in the atmosphere, *Physical Chemistry Chemical Physics*, *17*(27), 17914-17926,

doi:10.1039/C5CP02001H.

Paatero, P., and U. Tapper (1994), Positive matrix factorization: A non-negative factor model with optimal utilization of error estimates of data values, *Environmetrics*, *5*(2), 111-126, doi:10.1002/env.3170050203.

Paulot, F., J. D. Crounse, H. G. Kjaergaard, A. Kürten, J. M. St. Clair, J. H. Seinfeld, and P. O. Wennberg (2009), Unexpected Epoxide Formation in the Gas-Phase Photooxidation of Isoprene, *Science*, *325*(5941), 730-733, doi:10.1126/science.1172910.

Petit, J. E., O. Favez, A. Albinet, and F. Canonaco (2017), A user-friendly tool for comprehensive evaluation of the geographical origins of atmospheric pollution: Wind and trajectory analyses, *Environmental Modelling & Software*, *88*, 183-187, doi:http://dx.doi.org/10.1016/j.envsoft.2016.11.022.

Polissar, A. V., P. K. Hopke, and R. L. Poirot (2001), Atmospheric Aerosol over Vermont: Chemical Composition and Sources, *Environ. Sci. Technol.* , *35*(23), 4604-4621, doi:10.1021/es0105865.

Rattanavaraha, W., et al. (2016), Assessing the impact of anthropogenic pollution on isoprene-derived secondary organic aerosol formation in PM2.5 collected from the Birmingham, Alabama, ground site during the 2013 Southern Oxidant and Aerosol Study, *Atmos. Chem. Phys.*, *16*(8), 4897-4914, doi:10.5194/acp-16-4897-2016.

Riedel, T. P., Y.-H. Lin, S. H. Budisulistiorini, C. J. Gaston, J. A. Thornton, Z. Zhang, W. Vizuete, A. Gold, and J. D. Surratt (2015), Heterogeneous Reactions of Isoprene-Derived Epoxides: Reaction Probabilities and Molar Secondary Organic Aerosol Yield Estimates, *Environ. Sci. Technol. Lett.*, *2*(2), 38-42, doi:10.1021/ez500406f.

Riva, M., S. H. Budisulistiorini, Z. Zhang, A. Gold, and J. D. Surratt (2016), Chemical characterization of secondary organic aerosol constituents from isoprene ozonolysis in the presence of acidic aerosol, *Atmos. Environ.*, *130*, 5-13, doi:http://dx.doi.org/10.1016/j.atmosenv.2015.06.027.

St. Clair, J. M., J. C. Rivera-Rios, J. D. Crounse, E. Praske, M. J. Kim, G. M. Wolfe, F. N. Keutsch, P. O. Wennberg, and T. F. Hanisco (2016), Investigation of a potential HCHO measurement artifact from ISOPOOH, *Atmos. Meas. Tech.*, *9*(9), 4561-4568, doi:10.5194/amt-9-4561-2016.

Sun, Y., Q. Jiang, Z. Wang, P. Fu, J. Li, T. Yang, and Y. Yin (2014), Investigation of the sources and evolution processes of severe haze pollution in Beijing in January 2013, *J.*

*Geophys. Res. Atmos.,, 119*(7), 4380-4398, doi:10.1002/2014JD021641.

Sun, Y., Z. Wang, H. Dong, T. Yang, J. Li, X. Pan, P. Chen, and J. T. Jayne (2012), Characterization of summer organic and inorganic aerosols in Beijing, China with an Aerosol Chemical Speciation Monitor, *Atmos. Environ.*, *51*, 250-259, doi:10.1016/j.atmosenv.2012.01.013.

Surratt, J. D., A. W. H. Chan, N. C. Eddingsaas, M. Chan, C. L. Loza, A. J. Kwan, S. P. Hersey, R. C. Flagan, P. O. Wennberg, and J. H. Seinfeld (2010), Reactive intermediates revealed in secondary organic aerosol formation from isoprene, *Proc. Natl. Acad. Sci. U.S.A.*, *107*(15), 6640-6645, doi:10.1073/pnas.0911114107.

Surratt, J. D., et al. (2006), Chemical Composition of Secondary Organic Aerosol Formed from the Photooxidation of Isoprene, *J. Phys. Chem. A*, *110*(31), 9665-9690, doi:10.1021/jp061734m.

von Schneidemesser, E., P. S. Monks, V. Gros, J. Gauduin, and O. Sanchez (2011), How important is biogenic isoprene in an urban environment? A study in London and Paris, *Geophys. Res. Lett.*, *38*(19), doi:10.1029/2011GL048647.

Wang, J., T. B. Onasch, X. Ge, S. Collier, Q. Zhang, Y. Sun, H. Yu, M. Chen, A. S. H. Prévôt, and D. R. Worsnop (2016), Observation of Fullerene Soot in Eastern China, *Environ. Sci. Technol. Lett.*, *3*(4), 121-126, doi:10.1021/acs.estlett.6b00044.

Xiong, F., et al. (2015), Observation of isoprene hydroxynitrates in the southeastern United States and implications for the fate of NOx, *Atmos. Chem. Phys.*, *15*(19), 11257-11272, doi:10.5194/acp-15-11257-2015.

Xu, L., et al. (2015a), Effects of anthropogenic emissions on aerosol formation from isoprene and monoterpenes in the southeastern United States, *Proc. Natl. Acad. Sci. U.S.A.*, *112*(1), 37-42, doi:10.1073/pnas.1417609112.

Xu, L., et al. (2016), Enhanced formation of isoprene-derived organic aerosol in sulfur-rich power plant plumes during Southeast Nexus, *Journal of Geophysical Research: Atmospheres*, *121*(18), 11,137-111,153, doi:10.1002/2016JD025156.

Xu, L., S. Suresh, H. Guo, R. J. Weber, and N. L. Ng (2015b), Aerosol characterization over the southeastern United States using high-resolution aerosol mass spectrometry: spatial and seasonal variation of aerosol composition and sources with a focus on organic nitrates, *Atmos. Chem. Phys.*, *15*(13), 7307-7336, doi:10.5194/acp-15-7307-2015.

Zhang, Y., et al. (2015a), Chemical composition, sources and evolution processes of aerosol at an urban site in Yangtze River Delta, China during wintertime, *Atmos. Environ.*, *123*,

*Part B*, 339-349, doi:http://dx.doi.org/10.1016/j.atmosenv.2015.08.017.

Zhang, Y. J., et al. (2015b), Insights into characteristics, sources, and evolution of submicron aerosols during harvest seasons in the Yangtze River delta region, China, *Atmos. Chem. Phys.*, *15*(3), 1331-1349, doi:10.5194/acp-15-1331-2015.

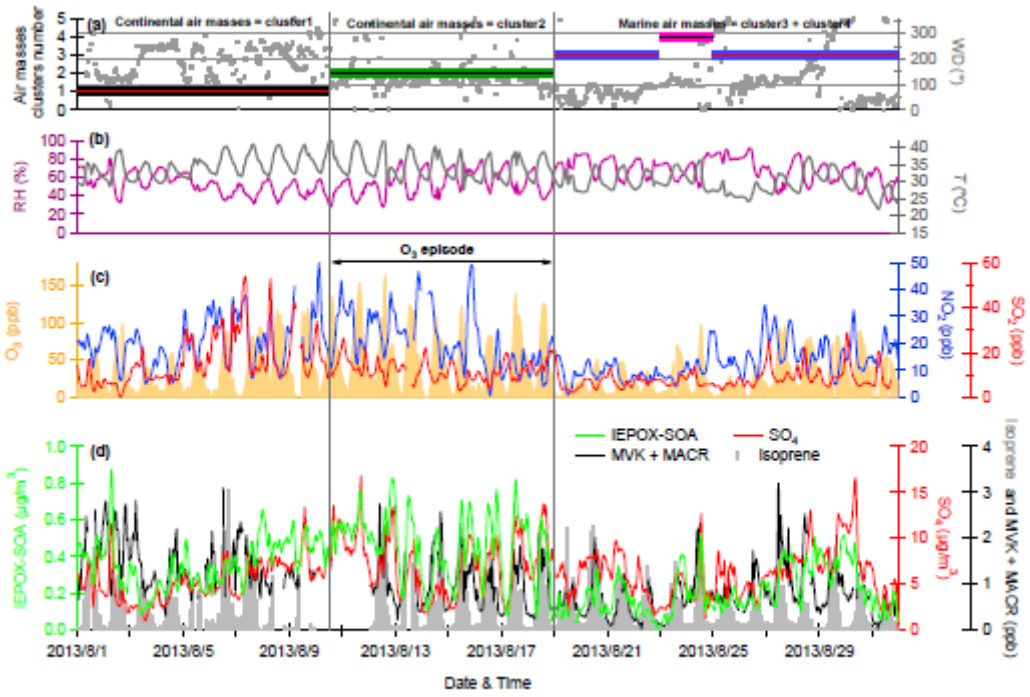


**Figure 1.** Time series of (a) wind direction (WD) (b) relative humidity (RH) and ambient temperature (*T*); (c) $O_x$ (= $O_3$ + $NO_2$), $NO_2$, and $SO_2$; and (d) mass concentrations of IEPOX-SOA, sulfate ($SO_4$), isoprene, and methyl vinyl ketone and methacrolein (MVK+MACR). The air masses during the study period were also classified into four clusters as shown in Figure S2. The missing data of isoprene and MVK+MACR on the Fig. 1d denotes instrument was not sampling ambient air.

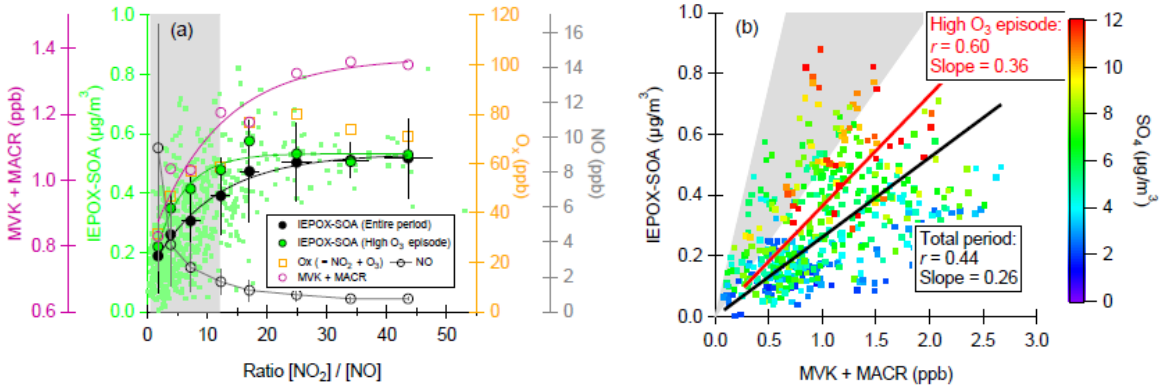


**Figure 2.** (a) Variations of IEPOX-SOA, MVK+MACR, Ox, and NO as a function of $[NO_2]/[NO]$ . The gray shaded area (a) represents the typical ratios of $[NO_2]/[NO]$ in summer in southeastern US [*Rattanavaraha et al.*, 2016; *Xu et al.*, 2015b]; and (b) IEPOX-SOA versus MVK+MACR, which are color coded by $O_x$ and $SO_4$, respectively. The gray shaded area (b) represents the typical ratios of [IEPOX-SOA] to [MVK+MACR] [*Budisulistiorini et al.*, 2015; *Xiong et al.*, 2015; *Xu et al.*, 2015a] under relatively low-$NO_x$ environments in summer 2013 in southeastern US. In addition, the correlations during high $O_3$ episode marked in Fig. 1 are also shown.

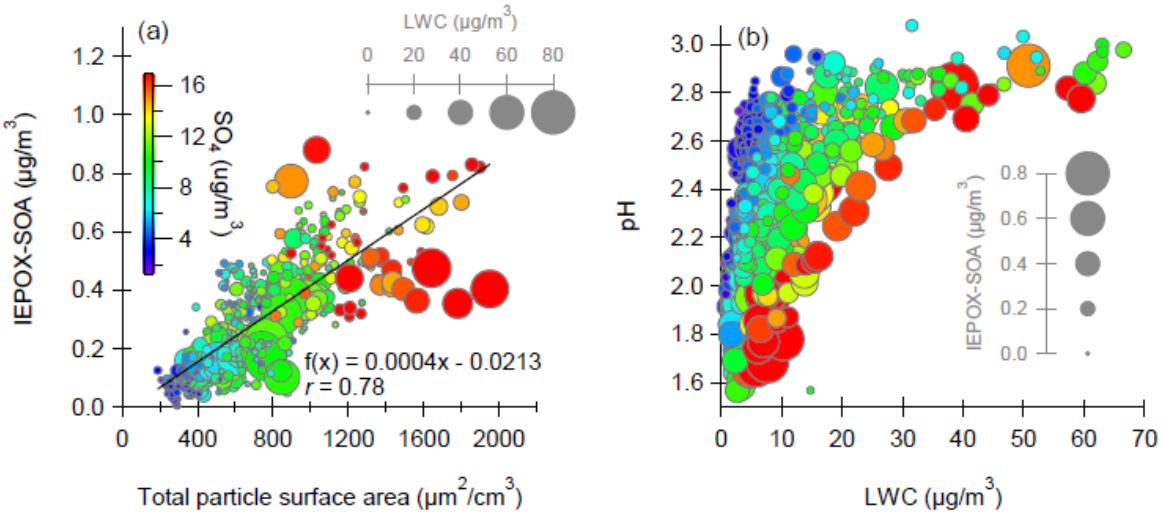


**Figure 3.** (a) Correlation between IEPOX-SOA and total particle surface area, and (b) relationship between aerosol particle pH and LWC. The data points in (a) and (b) are color coded by $SO_4$ concentrations, and the marker sizes indicate the values of LWC and IEPOX-SOA, respectively.

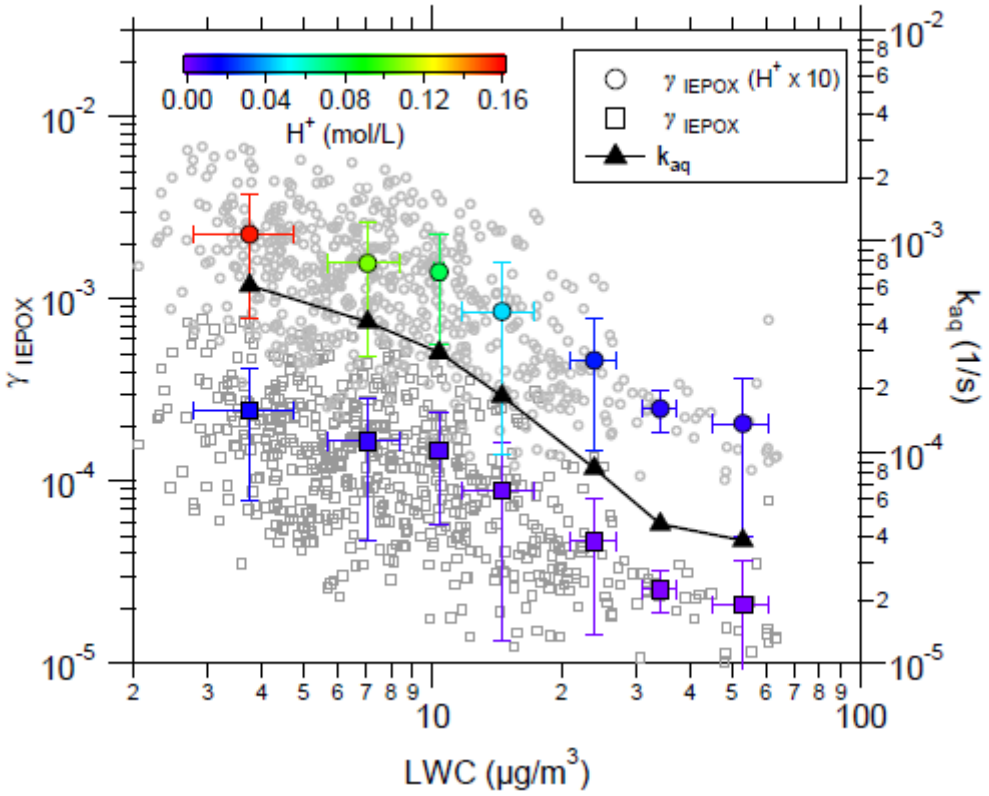


**Figure 4.** Reactive uptake ($\gamma_{IEPOX}$) and heterogeneous reaction rate constant ($k_{aq}$) of IEPOX as a function of particle LWC. Also, the data points colored by the aerosol acidity ($H^+$) were averaged into seven bins according to LWC.

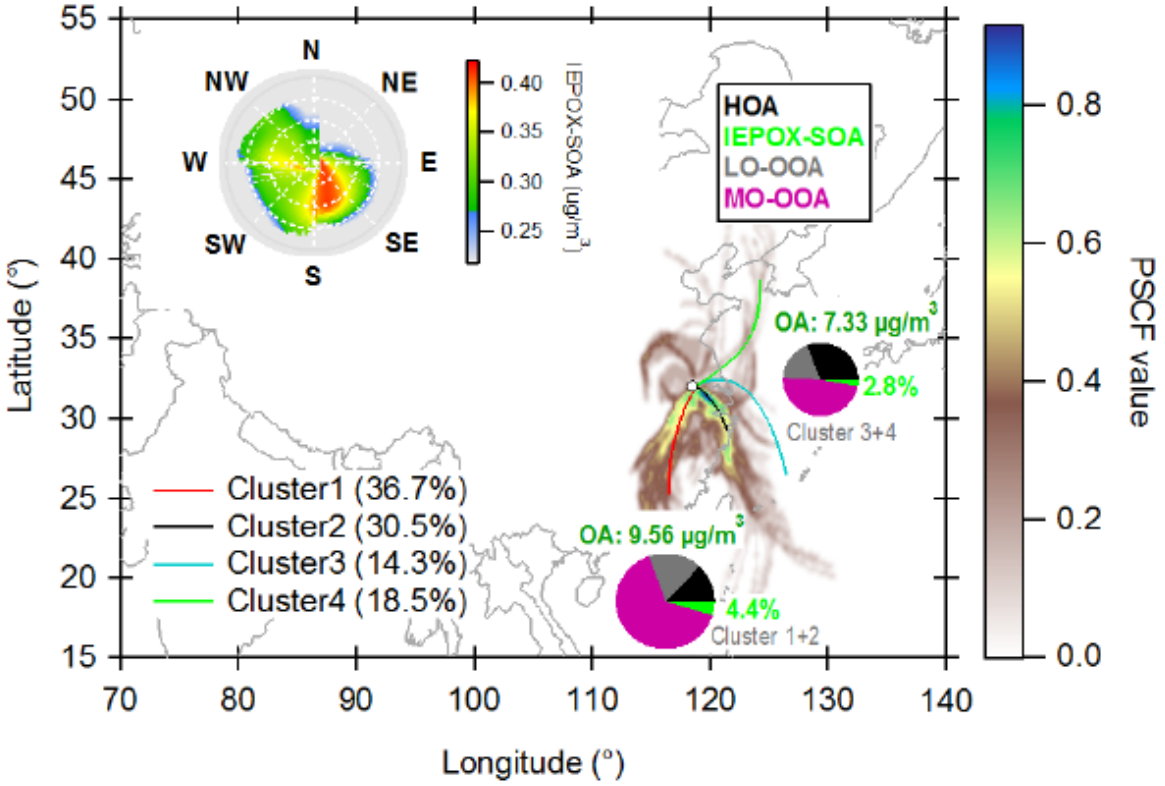


**Figure 5.** Potential source contribution function (PSCF) and NWR plots of IEPOX-SOA. The two pie charts show the average OA composition for cluster 1 and 2, and cluster 3 and 4.